

Material Forces: A Novel Approach to Fracture Mechanics in ANSYS



Durability and failure investigations of products are of high interest to determine the risk of failure in engineering applications. This white paper discusses features regarding the use of the novel material force approach in linear-elastic fracture mechanics (LEFM) and elastic-plastic fracture mechanics (EPFM). Although the main focus of the paper is on the material force method, a compact summary is given on general fracture mechanics.

Contents

Fundamentals

Overview
Mechanics in Material Space
Material-Force Concept
Material Durability and Fracture
Mechanics Approach
Linear-Elastic Fracture Mechanics Criteria
Elasto-Plastic Fracture Mechanics
Advantages of Material-Force Approach

How to Use the Material-Force Approach in ANSYS (Case Studies)

Plate with a Single Central Crack
Compact Tension Specimen
Two-Dimensional Specimen with Inclined Crack
Three-Dimensional Semi-Elliptical Surface Crack
Elasto-Plastic Compact Tension Specimen

Summary

Appendix

Theory
APDL Codes

Efficient and realistic analysis by using fracture mechanics based-design of products relies on several important aspects:

- Material behavior (linear or nonlinear, time-dependent, temperature a moisture effects, hysteresis due to plasticity or visco-elasticity, anisotropy, description of micro structure of constituent, etc.)
- Determination of material parameters from test data
- Definition of the term durability of a product (fracture-based fatigue or failure, stress-strain-based fatigue or failure, mechanics-based statistics of failure risk, etc.)
- Use of correct failure model and fracture parameter

ANSYS offers a well-balanced combination of a sophisticated analysis code to simulate material behavior and to evaluate fracture phenomena seamlessly with a user-friendly graphical user interface and APDL features. This makes ANSYS uniquely suitable for simulating complex physics of fracture phenomena. The material force approach is an advanced feature that is a more general and easy-to-use method to assess fracture mechanical criteria and the crack propagation direction. Material force evaluation is based on continuum mechanics and material force vectors that act on imperfections, discontinuities and dislocations. As an example, the material force can be imagined as a force-opening zipper (Figure 1.1) in a precracked structure. If the crack-driving force gets large enough to reach the critical value or the fracture toughness of the material, fracture occurs, and the crack propagates in the direction of the inverse of the crack-driving force at the sharp crack tip.

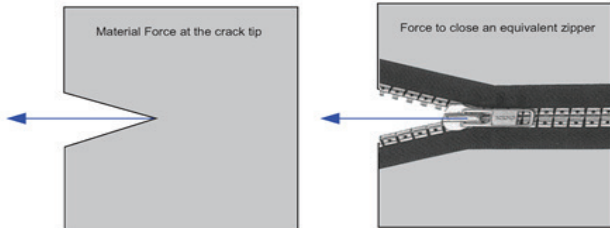


Figure 1.1. Schematic definition of crack tip material force to open equivalent zipper

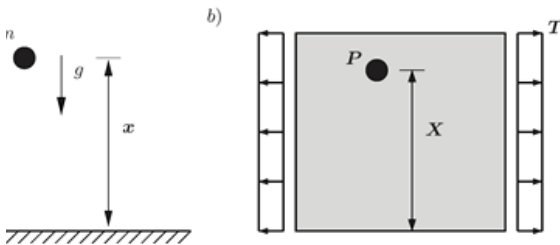


Figure 1.2. Schematic definition of physical and material spaces: a) mass under gravity in physical space; b) void or inclusion in solid in material space

1.2 Mechanics in Material Space

This section presents an overview of the concepts of classical mechanics in physical space and mechanics in material space based on the interpretation of Kienzler and Herrmann (2000). In classical mechanics, motion of objects is concerned with the equilibrium depending on the circumstances and goals of the mathematical modeling of realistic behavior of the solid obeying a variety of constitutive equations.

However, materials cannot be regarded as perfect continua because they contain a variety of defects and imperfections (as described in the previous section). Thus, it is necessary to deal with these imperfections and inhomogeneities, which may have mass like inclusions or may have no mass like voids. To characterize these inclusions or voids, the introduction of the concept of a force-like quantity in the material space must be introduced by analogy to the concept of the force acting in physical space. This step can lead to the construction of mechanics in material space.

To illustrate material forces in a simple body, it is necessary to describe differences between the basic fundamentals of the mechanics in the physical space and the material space. The physical space usually can be assumed to be Euclidean, homogeneous and not changing in time. To give an example, if a particle of mass m at distance x under a gravity field g is assumed in the physical space as shown in Figure 1.2a, the total potential is $\Pi = mgx$ and the physical force action on the mass has form

$$F = -\frac{\partial \Pi}{\partial x} \tag{1.1}$$

On the other hand, in the material space, the solid can be assumed to be not homogeneous, anisotropic and possibly changing in time. For instance, if an elastic plate, which contains a defect or an inclusion P at the position X , subjected to traction T is assumed as shown in Figure 1b, the total energy \mathcal{I} can be written as a function of several quantities α_i and the position in the material space X as $\Pi = \Pi(\alpha_i, X)$. Consequently, the force F acting on the defect reads

$$\mathcal{F} = -\frac{\partial \Pi}{\partial X} \tag{1.2}$$

Here, \mathcal{F} is called “material force.”

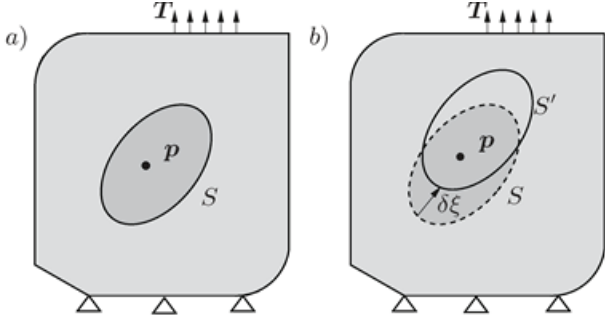


Figure 1.3. Eshelby's thought experiment: a) original system with inclusion surrounding surface S; b) replicated system with surrounding surface X moved by $\delta\xi$

Following Eshelby's thought experiment, the computation of the material force on a defect in an elastic medium can be derived by using the so-called energy momentum tensor. To this end, an externally loaded linear-elastic body containing a defect or an inclusion enclosed by the surface S is considered. Then, S is moved to S' by an infinitesimal displacement $\delta\xi$ in a replica body, and the same load is applied, as shown in in Figure 1.3. Eshelby investigated the energy change associated with change of the position of the bodies S and S'. Finally, he introduces the energy change as

$$\delta\Pi = -\delta\xi \int_S [\Psi\mathbf{1} - \nabla\mathbf{u}^t\boldsymbol{\sigma}]n dA, \quad (1.3)$$

in which n is the outward unit normal to S, Ψ is the internal strain energy function of the solid, $\boldsymbol{\sigma} = \partial_e\Psi$ is the Cauchy stress tensor, and $\nabla\mathbf{u}$ is the gradient of the displacement field. If we consider the energy change $\delta\Pi$ is a priori as a scalar product of material force F with the infinitesimal displacement $\delta\xi$, the above equation can be recast into the form

$$\delta\Pi = \delta\xi\mathcal{F} \quad (1.4)$$

The combination of the last two equations yields the material force F as an integral taken over the closed surface S

$$\mathcal{F} = - \int_S \boldsymbol{\Sigma}n dA, \quad (1.5)$$

with $\boldsymbol{\Sigma} = \Psi\mathbf{1} - \nabla\mathbf{u}^t\boldsymbol{\sigma}$ as energy momentum tensor. Today, it is also called the Eshelby tensor.

1.3 Material-Force Concept

To interpret the material-force approach, the difference between the concepts of physical forces and material forces should be nonambiguous. The physical force concept, which can be traced back to Newton and Galilei, describes the relation between physical forces and corresponding deformations of bodies in the physical space to investigate quantities during continuum and structural mechanical investigations. However, in fracture mechanics, issues addressing discontinuities, cavities, flaws and inhomogeneities can be described only with additional physical and mathematical

concepts. Based on mechanics in the material space, a concept of material forces can be interpreted as force vectors acting on imperfections and dislocations, such as:

- Discontinuities
 - Voids
 - Cavities
 - Cracks
 - Inclusions
- Imperfection in crystals and micro-structures
 - Foreign atoms
 - Grain boundaries
- Physical inhomogeneities
 - Material inhomogeneities
 - Elastic-plastic zone transition
 - Transition zone in bimaterial
- Numerical inhomogeneities
 - Mesh inconsistency in the finite element method (FEM)

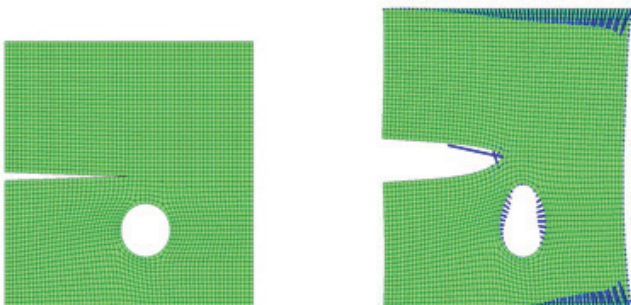


Figure 1.4. Distribution of material forces in precracked plate with hole

To illustrate the evaluation of material forces after a finite element solution, a plate under tension with an initially circular hole and an initial crack is presented in Figure 1.4. The distribution of material forces is plotted. As it is described above, large material forces exist at the crack tip and around the hole, which can be interpreted as a void. Here, the crack tip material force can be interpreted as a crack-driving force. In addition, material forces appear at the external boundaries, however such boundary material forces are not related to crack-driving force.

In this white paper, section 1 includes a general overview on the fracture mechanics-based theory of material durability. Section 2 provides compact information about numerical solution strategies of the material-force approach. Section 3 validates the discussion with the help of representative numerical examples. Section 4 includes concluding remarks and comments.

1.4 Material Durability and Fracture Mechanics Approach

Increasing the fatigue life and service time of a product decreases waste and saves resources. Therefore, you must define the term durability of a material or a product in order to optimize it. A reliable failure predictor could be used to define the component's life cycle, which is of great interest for engineering. A main goal of using ANSYS® software for fracture mechanics investigations of structures is to evaluate durability features of a structure.

One of the primary goals of fracture mechanics as an engineering discipline is related to investigating structures with existing flaws as well as the propagation of cracks under ultimate or fatigue loading. Therefore, information required to enable durability prediction like crack initiation, crack propagation and crack direction can be taken into consideration by using fracture mechanics. The pioneering contribution of Griffith in the 1920s was related to infinite stress values at a cracked plate. Griffith was the first who realized the importance of the variation of energy during crack advancement in brittle solids. He proposed that solids have a surface energy, which must be released during crack propagation. Then, the critical load level for a given crack is found by the principle of minimum potential energy with a crack extension that can be assumed as the surface energy of the solid. In other words, Griffith's basic idea is the formulation of an energy-balance approach as the critical condition of fracture. He postulates that there is an inherent resistance to crack growth on one side and a crack-driving force resultant from the potential energy release on the other side. The corresponding equilibrium condition is given as

$$\frac{d\Psi}{dA} - \frac{dW}{dA} = -\frac{d\Pi}{dA} = \frac{d\Gamma}{dA} \quad (1.6)$$

for an elastic material. This equation relates potential energy changes Π , consisting of internal strain energy Ψ and external work W contributions. The crack surface energy at incremental crack growth is Γ . The physical interpretation provides a variation between potential energy during crack propagation, which is the work required to create new surfaces. The introduction of the left part of equation (1.6) as energy release rate

$$G = \frac{d\Psi}{dA} - \frac{dW}{dA} = -\frac{d\Pi}{dA} \quad (1.7)$$

gives a measure of the available energy to create a new surface or, rather, crack propagation. The terminology of rate is used in this context for the change of $d\Pi$ caused by an incremental change of the crack area dA . Alternatively, the notation of G as force (for example, crack-driving force or more-general thermodynamic-driving force) is used with respect to the derivation of a potential and the resultant measurement. The introduction

of the material surface energy γ and the relation between the crack area and fracture energy changes

$$d\Gamma = \dot{\Gamma}dt = 2\gamma dA \quad (1.8)$$

enables to rewrite the formulation of equation (1.6). The distinction between crack area and surface area introduces the factor of two. While the first one is defined as the projected area of the crack, the increase of the generated surfaces due to crack propagation consists of two mutual surfaces. The critical condition of crack propagation

$$G_c = 2\gamma \quad (1.9)$$

is valid for an elastic-brittle material under quasi-static and stable crack propagation. The parameter G_c represents the material's resistance (toughness) to crack advancement under stable crack-growth condition or a structural failure under unstable crack-growth condition, which essentially refers to critical energy release rate. Due to the irreversible nature of fracture processes, the rate of fracture energy Γ always yields positive values.

1.4.1 Linear-Elastic Fracture Mechanics Criteria

Further developments on fracture mechanics are related to a lack of Griffith's energy theory. The neglect of stresses due to surface energy dissipation, the omitted consideration of combined stress conditions, and the incomplete description of continued crack growth are examples for such deficiencies. Moreover, the necessary computation of potential energy changes for specified crack stages makes practical applications expensive. Irwin (1957) introduced a quantitative relation between the global energy release rate G and the intensity of the local stress field in terms of stress intensity factors K_i in dependence on the crack opening Mode I. The linear elastic stress and strain field around the crack tip are characterized by the stress intensity factor

$$K = K(\sigma, a, f(\beta)) \quad (1.10)$$

in dependence on the applied load σ , the length of the crack a and another function $f(\beta)$, which depends on dimensions of the specimen or structure. Three basic modes of crack propagation

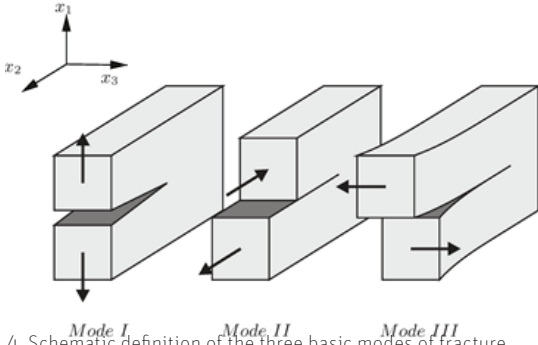


Figure 1.4. Schematic definition of the three basic modes of fracture

were first pointed out by Irwin. The modes are based on the movements of two crack surfaces with respect to each other. As shown in Figure 1.5, the three modes are summarized here:

- Mode I (pure opening): The applied load is normal to the crack surfaces separate such that, $\llbracket u_1 \rrbracket \neq 0$, $\llbracket u_2 \rrbracket = \llbracket u_3 \rrbracket = 0$.
- Mode II (sliding/in-plane shear): The applied load is parallel to the crack plane corresponding to in-plane shear loading and the crack surfaces separate such that, $\llbracket u_2 \rrbracket \neq 0$, $\llbracket u_1 \rrbracket = \llbracket u_3 \rrbracket = 0$.
- Mode III (out-of-plane shear): The applied load is parallel to the crack plane corresponding to an out-of-plane shear loading and the crack surfaces separate such that, $\llbracket u_3 \rrbracket \neq 0$, $\llbracket u_1 \rrbracket = \llbracket u_2 \rrbracket = 0$.

The jump bracket $\llbracket u_{i=1\dots 3} \rrbracket$ is employed above to illustrate the difference of the displacement component u_i evaluated at both faces of the crack. That is with the displacement values at the upper and lower crack faces and, respectively.

Two fundamental terms, the stress intensity factor K_i and the strain energy release rate G , can be employed to describe the fracture criterion. The stress intensity factor K_i describes the intensity of stress and strain fields near the crack tip. Similarly, the parameter G describes the rate of the variational energy associated with an increment of crack extension. Therefore, it is possible to come to the conclusion that the stress intensity factor is a local parameter, while the energy release rate describes the global behavior. The relation between the strain energy release rate and the stress intensity factor can be derived for a linear-elastic solid under pure Mode I loading as follows:

$$G_I = \frac{K_I^2}{E'} \quad (1.11)$$

Here, for plane-strain and 3D stress state conditions, E' must be replaced by $E/(1-\nu^2)$ and for plane stress conditions, E' is equal to E . Here, E and ν are the modulus of elasticity and Poisson's ratio, respectively. The three modes of fracture are illustrated in the Figure 1.5, the particular relations

$$G_{II} = \frac{3-\nu}{8(1+\nu)} \frac{K_{II}^2}{\mu} \quad \text{and} \quad G_{III} = \frac{1}{2} \frac{K_{III}^2}{\mu} \quad (1.12)$$

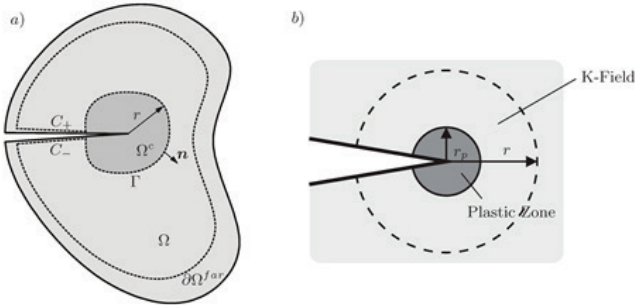


Figure 1.6. Two-dimensional precracked domain with a) subdomain, b) visualization of plastic zone in a two-dimensional precracked domain

are applicable for pure Mode II and Mode III problems in which μ is the shear modulus. For the general case of mixed crack loading,

$$\mathcal{G} = \frac{K_I^2 + K_{II}^2}{E'} + \frac{1}{2} \frac{K_{III}^2}{\mu} \quad (1.13)$$

gives the energy release rate. These relations between the energy value \mathcal{G} and the local stress-based parameters K_I , K_{II} and K_{III} , which is available for a wide range of structural problems, significantly improved the application of fracture mechanics in engineering practice.

1.4.2 Elasto-Plastic Fracture Mechanics Criteria

In general, real materials show dissipative effects due to inelasticity. Since stress fields for stationary cracks are not valid anymore, stress intensity factors loose their meaning. In other words, the elastic stress analysis becomes inaccurate as the plastic region at the crack tip increases. Simple corrections to LEFM are available when fracture process zones are small enough to be ignored. The size of the fracture process zone can be estimated by Irwin's approach, in which elastic stress analysis is used to estimate the elastic-plastic boundary. The approach leads to simple corrections for crack-tip yielding. The range of a valid description is bounded by the radius r as shown in Figure 1.6b. Due to the singular nature of the elastic description and the restriction of an ultimate material strength σ_y , the K-dominated zone has also an internal radius r_p . Here, the material behavior is governed by inelastic deformations in terms of elasto-plasticity. For the assumption of a large K-dominated zone in relation to the inelastic zone $r_p \ll r$, the idea of a fully K-governed crack tip stays valid. Therefore, LEFM stays valid and applicable. The approximate size of r_p is given by the equation of the stress field σ and the yield stress of the material σ_y and results in

$$r_p = \frac{1}{n\pi} \frac{K_I^2}{\sigma_y^2} \quad (1.14)$$

under a pure Mode I loading, with $n=1$ for plane stress and $n=3$ for plane-strain idealization. As mentioned above, the description of a fracture process within the regime of LEFM becomes inapplicable when the crack tip field is characterized by a significant amount of inelastic deformations. Another concurrent approach was established by Wells (1963) with the crack tip opening displacement (CTOD) as the governing parameter for crack extension as well as crack tip opening angle (CTOA).

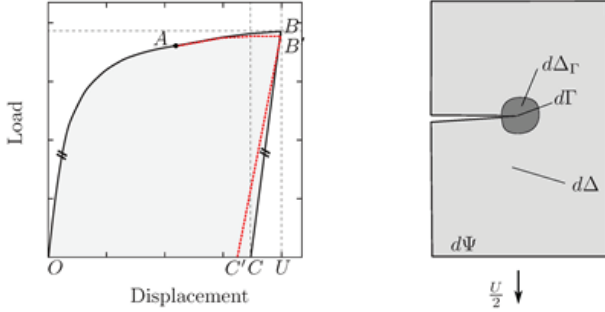


Figure 1.6. Two-dimensional precracked domain with a) sub-domain, b) visualization of plastic zone in a two-dimensional precracked domain

From an energy evaluation point of view, energy partitioning in a cracked body can be investigated. To this end, Figure 1.7 represents schematic diagrams of the relevant test information for a center-cracked elasto-plastic sheet-loaded-displacement-controlled up to maximum displacement U and unloaded completely. Referring to Figure 1.7a, it can be assumed that point A designates an arbitrary point on the nonlinear part of the load displacement curve for a specimen with a crack in a fixed configuration. In the absence of crack growth, OABC and BCU designate the nonrecoverable and recoverable parts, respectively, of the displacement U . The total strain energy of deformation must be equal to the work of the applied force and, thus, must also be equal the area under the OABU curve. We require the derivatives of the above energy quantities at the onset of crack extension. To obtain such derivatives, one may consider these quantities after an arbitrary small imagined increment of crack growth ΔA that, for convenience, is taken under displacement-controlled loading condition. Thus, with crack extension, global stiffness reduction takes place and the load displacement curve acquires a different character as OAB'U. With this assumption from experimental evidence at hand, we can rewrite the incremental energy balance $\Pi = OABU - OAB'U$ for an inelastic body as

$$d\Pi = d\Psi - dW = d\Gamma + d\Delta + d\Delta_{\Gamma} \quad (1.15)$$

Here, $d\Delta_{\Gamma}$ presents the energy dissipated by material inelasticity in a fracture process zone, or rather singular zone, whereas $d\Delta$ represents the energy dissipation in the rest of the body. The illustration of the terms above is presented in Figure 1.7b. Accordingly, the energy release rate can be written as

$$G = \frac{d\Psi}{dA} - \frac{dW}{dA} = \frac{d\Delta}{dA} + \frac{d\Delta_{\Gamma}}{dA} + \frac{d\Gamma}{dA} = -\frac{d\Pi}{dA} \quad (1.16)$$

By comparison of equations (1.16) and (1.7), it can be interpreted that the energy dissipation of inelastic materials contributes to the crack-growth resistance. However, in fracture mechanics, a specific criterion is required that governs crack growth. With the definition in equation (1.16), the so-called crack-driving force can be identified as

$$\frac{d\Gamma}{dA} = \frac{d\Psi}{dA} - \frac{dW}{dA} - \frac{d\Delta}{dA} - \frac{d\Delta_{\Gamma}}{dA} \quad (1.17)$$

1.5. Advantages of the Material-Force Approach

The main advantage of using the material-force approach is that it can be adapted to all kind of material models (elastic, finite elastic, visco-elastic, plastic, coupled mechanics, etc.) in which the material response is explicitly defined by a strain energy density function. The method provides expressions for the global material and dissipation forces that yield the near-tip crack-driving force. Although traditional methods have been used commonly to evaluate fracture criteria successfully in ANSYS software, because of the vectorial nature of the material force and its capability of use for a large class of material models, it became one of the most interesting methods in fracture mechanical investigations.

The most commonly used methods to evaluate fracture criteria, which are available in ANSYS, are the displacement extrapolation method (DEM), the virtual crack closure method (VCCT) and the J-integral. Since, the concept of J-integral is indeed directly related to material forces, it is crucial to outline the difference between the material force approach and the J-integral proposed by Rice (1968). We consider a two-dimensional homogeneous linear or nonlinear elastic solid free of body forces. The body contains a plane crack in which the crack surfaces are parallel to each other, as shown in Figure 1.6. The traditional J-integral is defined by

$$\mathcal{J} = \int_{\Omega^c} [(\mathcal{W} - \sigma \nabla \mathbf{u}) \mathbf{n}] dV, \quad (1.18)$$

In which Ω^c is an arbitrary path that surrounds the crack tip running counterclockwise from the lower flat notch surface to the upper one (Figure 1.6). The vector \mathbf{n} denotes the unit outward normal to the path, while $\nabla \mathbf{u}$ is the deformation gradient. In general, J-integral gives the energy flux to the crack tip. Therefore, in LEFM, the material-force approach and the traditional J-integral coincide, and they give the energy needed to create a new free surface. In this case, the main difference between the material-force approach and J-integral is the integration algorithm. For material forces, the integration yields vectorial nodal values, whereas the J-integral gives a scalar quantity with a surface or volume integration. Since the material-force approach offers a vectorial criterion and lets the user visually evaluate the singularity, it should be preferred over other methods. Moreover, the material force can directly be used without an additional effort in nonlinear elasticity. Implementing the material force approach is extremely simple in three- or two-dimensional cases because of its node-based evaluation.

In materials in which material dissipation takes place, like plasticity, visco-elasticity etc., the J-integral uses the stress work density W in the integration, in which

$$\mathcal{W} = \int_0^t \sigma_{ij} \dot{\epsilon}_{ij} dt. \quad (1.19)$$

Therefore, for the J-integral, monotonic loading is required. In the material-force approach, it is not necessary to fulfill this requirement. In other words, the material-force approach is not only applicable to a large class of material models, but it is applicable to structures under complex loading and unloading scenarios.

The theory of material forces may be used for improving numerical solutions obtained by the finite element method. For instance, adaptive mesh refinement, in which the magnitude of the material forces acts as an indicator for mesh optimization, has been being used with great success for a variety of applications.

How to use the Material-Force Approach in ANSYS (Case Studies)

2.1 Plate with a Single Central Crack

As a first case study, a simple central cracked plate specimen, one of the most investigated examples in literature, is considered from the fracture mechanics point of view. The specimen consists of a block of homogeneous material, which is loaded by stress $\sigma=0.5641895$ psi (0.00388995 MPa) on its top side (Figure 2.1). Linear elastic material properties with the elastic modulus $E=30e6$ psi (206842.72 MPa) and Poisson's ratio $\nu=0.3$ are used. Dimensions of the specimen are $H=W=5$ in (127 mm), $a=1$ in (25.4 mm), and $t=0.25$ in (6.35 mm). Energy release rates are calculated by the material-force approach and compared to the theoretical result for plane-strain and three-dimensional cases.

Table 2.1. Central cracked plate specimen with PLANE183

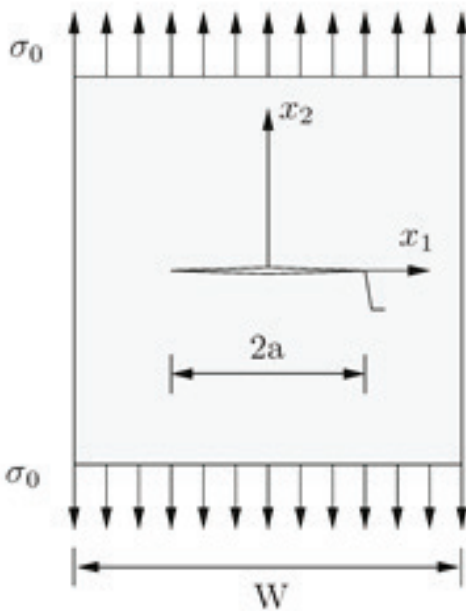


Figure 2.1. Infinite plate of unit thickness with a sharp crack of length $2a$ under remote stress σ_0 .

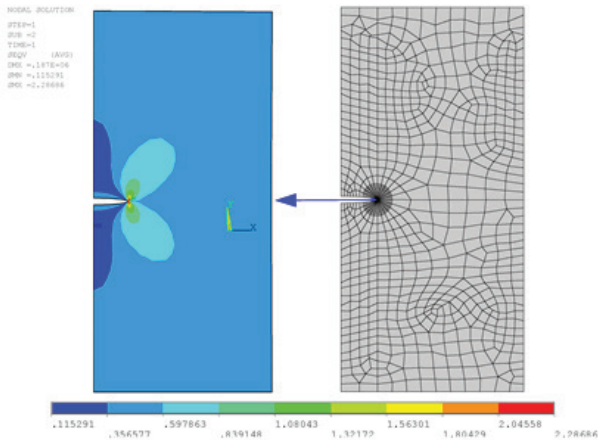


Figure 2.2. Two-dimensional central crack specimen: VonMises stress (left) and nodal material-force distribution (right)

The problem is solved first using the two-dimensional PLANE183 element with plane-strain behavior. After the pre-process (/PREP7) part of the APDL code, the crack-tip node or nodes can be introduced in the solution part (/SOLU) with CINT command as follows:

```
CINT,NEW,1
CINT,TYPE,MFOR
CINT,CTNC,CNodeComp
CINT,NCON,NumCon
CINT,NORM,0,2
CINT,SYMM,OFF
```

Here, CNodeComp is the node component at the crack tip and NumCon is the number of the integration contours. To get the results, PRCINT command can be used as

```
PRCINT,2,,MFRX
PRCINT,2,,MFRY
```

Since the crack normal is introduced as the second component of the global basis vector with the command CINT,NORM,0,2, the first command gives the tangential component of the material force, whereas the second one is the normal component to the crack surface. Since the problem is two-dimensional, CNodeComp includes only the crack-tip node. In Figure 2.2, von Mises stresses and nodal material force vectors are shown. High stress concentration occurs around the crack tip. Since there is a $r^{-0.5}$ stress singularity at the crack tip, the discrete material forces mainly appear in the crack-tip domain. The tangential component of the material-force vector to the crack surface presents the required energy to create a new crack surface. In other words, if the energy release rate or crack-driving force are large enough to outweigh fracture toughness of the material, the crack will propagate in the opposite direction of the material force as it is introduced in brittle fracture theory. The domain evaluation can be obtained by considering a resultant configurational force vector of an influence domain that surrounds the crack tip. In ANSYS software, this procedure can be accomplished by contours. The user-defined contour, by the command CINT,NCON,NumCon, represents domain evaluation. The first contour presents the individual

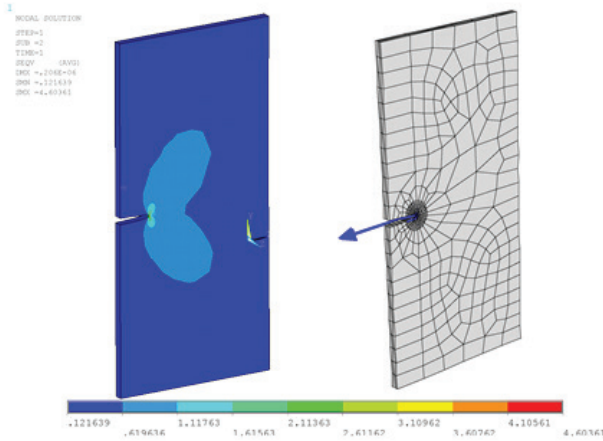


Figure 2.3. Three-dimensional central crack specimen: von Mises stress (left) and nodal material force distribution (right)

material force at the crack tip node where subsequent contours take the resultant material-force vectors from the neighboring nodes into the calculation. As shown in Table 2.1, the crack-tip material force, which is equal to the first domain result from the material-force calculation by ANSYS software, gives more than 90 percent of the total energy release rate for this example.

In addition to the single-edge crack problem under plane-strain condition, the same problem is studied for the three-dimensional case. The same APDL commands are used as explained above. The nodal von Mises stress contour and nodal material force distribution can be found in Figure 2.3. Results are presented in Table 2.2 with a comparison to the ANSYS J-integral tool.

2.2 Compact Tension Specimen

In a second case study, a two-dimensional plane-strain model is analyzed in ANSYS. The specimen is loaded by applying a force to the pins in a vertical direction, as shown in Figure 2.4. The elastic modulus of the specimen's material is $E=213$ GPa, and Poisson's ratio is $\nu=0.3$. The geometry of the model is shown in Figure 2.4. The dimensions are given as thickness $t=25$ mm, width $W=62.5$ mm, $B=50$ mm, $H=60$ mm, and crack length $a=25$ mm. Since the crack-tip element degeneracy allows different singularity types to be defined, quarter-point singular elements are used to define crack-tip singularity, just as in the previous case study. Furthermore, APDL commands are used as

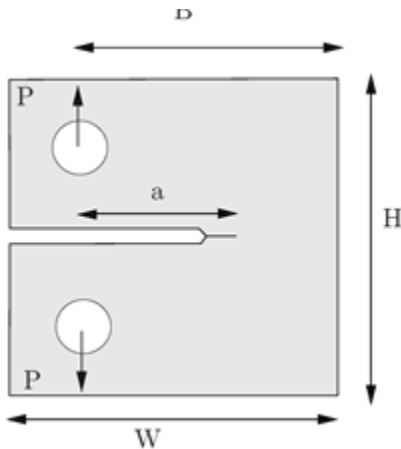


Figure 2.4. Schematic compact tension specimen loaded by force P

```
CINT,NEW,1
CINT,TYPE,MFOR
CINT,CTNC,CNodeComp
CINT,NCON,NumCon
CINT,NORM,0,2
CINT,SYMM,OFF
```

Von Mises stresses and the initial distribution of material forces F are plotted in Figure 2.5. In the close vicinity of the crack tip, spurious material forces occur due to the singularity of the crack-tip domain. If there is an additional singularity, such as non-optimal mesh design, transition zone between two different materials, other cracks, etc., an additional nodal material-force vector or vectors can appear. These material-force vectors should be excluded from the energy release rate evaluation, since they are not related to the crack-tip singularity. If these material forces are found due to non-optimal mesh, they can be used to adapt meshes to minimize spurious material forces.

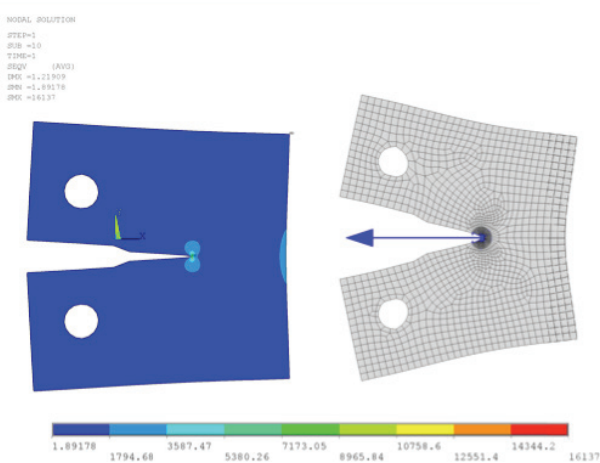


Figure 2.5. Two-dimensional compact tension specimen: von Mises stress (left) and nodal material force distribution (right)

Von Mises stresses and the initial distribution of material forces F are plotted in Figure 2.5. In the close vicinity of the crack tip, spurious material forces occur due to the singularity of the crack-tip domain. If there is an additional singularity, such as non-optimal mesh design, transition zone between two different materials, other cracks, etc., an additional nodal material-force vector or vectors can appear. These material-force vectors should be excluded from the energy release rate evaluation, since they are not related to the crack-tip singularity. If these material forces are found due to non-optimal mesh, they can be used to adapt meshes to minimize spurious material forces.

The results obtained from the material-force tool in ANSYS software are compared to the results computed according to the method used by ASTM (1996). Figure 2.6 plots the loading force versus the energy release rate results obtained by the two methods. The results obtained from ANSYS software are in very good agreement with the results obtained by the method described in ASTM.

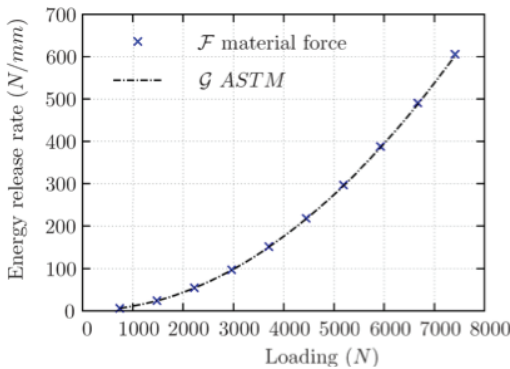


Figure 2.6. Energy release rate obtained by material-force approach for third contour versus the loading

2.3 Two-Dimensional Specimen with Inclined Crack

Figure 2.7 illustrates a general scenario for an inclined crack under remote stress. When failure occurs, the crack tends to propagate orthogonal to the applied normal stress in which the mixed-mode crack tries to obtain a pure Mode I loading. A propagating crack seeks the path of least resistance (or the path of maximum driving force). In other words, if the material is isotropic and homogeneous in the inclined crack problem, propagation will follow the path in a way that maximizes the energy release rate. In this case, the evaluation of the energy release rate can be computed as a function of propagation direction in mixed-mode problems. In this example, Mode I and Mode II are considered, but the basic methodology can, in principle, be applied to a more general case in which all three modes are present.

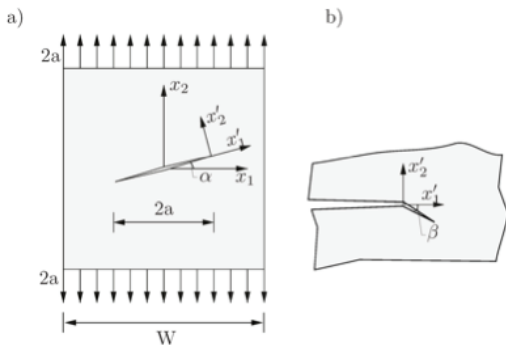


Figure 2.7. a) Infinite plate of unit thickness with inclined crack of length $2a$ under mixed-mode loading; b) schematic view of crack tip kink

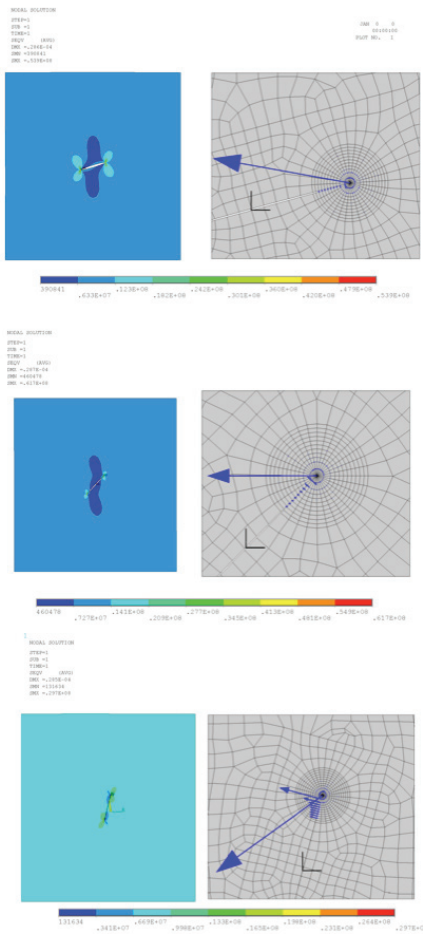


Figure 2.8 presents von Mises stress distribution and nodal material force vectors F in the inclined crack specimen with crack orientation angle $\alpha=15^\circ, 45^\circ$ and 75° , respectively. APDL command for material-force calculation is introduced as follows:

```

CINT,NEW,1
CINT,TYPE,MFOR
CINT,CTNC,CNodeComp
CINT,NCON,NumCon
CINT,NORM,11,2
CINT,SYMM,OFF
    
```

Here, unlike the previous case studies, the crack normal is the second component of the local basis vector, described in Figure 2.7. It is introduced with the command *CINT,NORM,11,2*. Figure 2.9 is a plot of the energy release rates for two different modes, Mode I and Mode II, versus crack-inclined angle α , as seen in Figure 2.7b. Energy release rates are calculated by the material force approach and VCCT. Results are compared to analytical ones. Material force results describe the total energy release rate $F_{x_1} = G_I + G_{II}$. Although it is not explicitly possible to separate G_I and G_{II} , the non-tangential component of the material-force vector to the crack surface can be interpreted as the sensitivity to crack deflection in terms of energy as $\mathcal{F}_{x_2} = \frac{\partial G}{\partial \beta}$, which β is the crack-kinking angle.

Figure 2.8. Two-dimensional specimen with inclined crack with crack orientation angles $15^\circ, 45^\circ$ and 75° : von Mises stress (left) and nodal material force distribution (right)

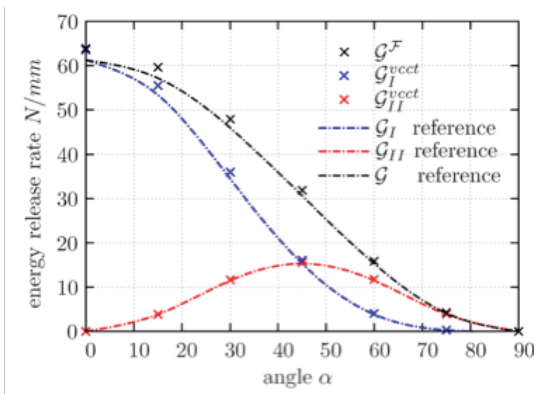


Figure 2.9. Energy release rate obtained by material-force approach and VCCT versus crack orientation angle (α)

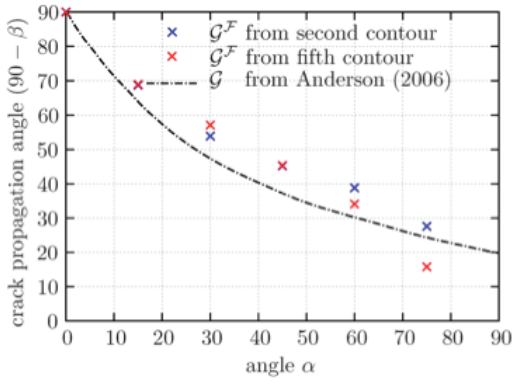


Figure 2.10. Crack propagation angle (90-β) versus crack orientation angle (α).

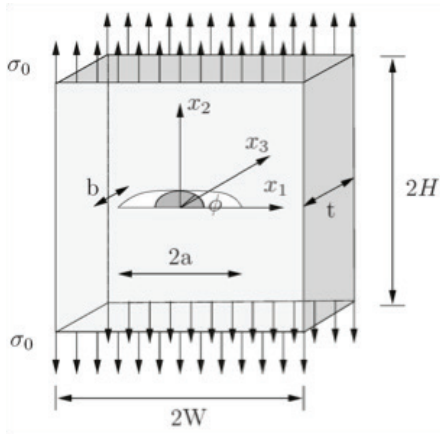


Figure 2.11. Infinite plate with semi-elliptical surface crack of length 2a under tension loading

Figure 2.10 shows the plots of the crack orientation angle α versus the kinking angle β , which are calculated by the inverse direction of the material force and taken from the function introduced in Anderson (2006). The dashed line represents the function that is calculated analytically according to the theory that the new crack surface will propagate in a direction to where the new surface will be under pure Mode I loading. The crosses show the directions that are obtained by the material-force approach evaluation from the second contour and fifth contour. As a result, we can come to the conclusion that the inverse direction of the material force describes successfully the crack propagation direction.

2.4 Three-Dimensional Semi-Elliptical Surface Crack

In this case study, the results of a semi-elliptical crack analysis under Mode I loading are compared to analytical solutions. Figure 2.11 illustrates the problem of an embedded elliptical crack in a three-dimensional block subject to a tensile stress. The representative sizes H and W are five times longer than the crack size a . Figure 2.12 presents the finite element model for the crack analyses. The analyses were carried out using the symmetry of the problem. The aspect ratio b/a of the crack is set to be 0.2, where b/t is set to be 0.2, 0.4 and 0.6. The size of the crack-front element in the case of the elliptical crack gradually changes along the crack front. The stress intensity factor is computed by assuming plane-strain condition. The stress intensity factor is normalized by the shape factor

$$K^n = \frac{K}{\sqrt{\frac{a}{Q}} \sigma_0}, \quad (2.1)$$

in which $Q=1.146$, as given in Newman and Raju (1984). APDL commands to enable material-force calculation are used as follows:

```
CINT,NEW,1
CINT,TYPE,MFOR
CINT,CTNC,CNodeComp
CINT,NCON,NumCon
CINT,NORM,0,2
CINT,SYMM,ON
```

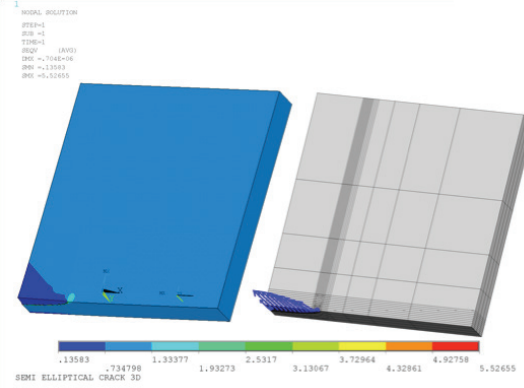


Figure 2.12. Von Mises stress and nodal material-force distribution in infinite plate with semi-elliptical surface crack of length $2a$.

Figure 2.12 presents von Mises stresses and distribution of material forces. The stress intensity factor solutions of the energy release rate with the material-force approach are presented in Figure 2.13. Notice that the computed stress intensity factor by the material force approach is in good agreement with the analytical values that are taken from the technical report published by Raju.

2.5 Elasto-Plastic Compact Tension Specimen

In this section, we discuss a cracked compact tension specimen with elasto-plastic material behavior under Mode I loading. The experimental part of the study is taken from the work of Simha et al. (2008). The dimensions are given as thickness $t=25$ mm, width $W=50$ mm, and crack length $a=25$ mm. The material is St37 type of mild steel with the Young's modulus $E=207$ GPa and Poisson's ratio is $\nu=0.3$, where the yield stress and ultimate stress are $\sigma_y = 270$ MPa and $\sigma_u = 426$ MPa, respectively. We used the well-known Voce hardening law in which yield function is introduced as

$$\phi = \|\sigma^{dev}\| - \sqrt{\frac{2}{3}}(\sigma_0 - R), \text{ where } R = R_0 e^{pl} + R_\infty(1 - e^{-b\epsilon^{pl}}) \quad (2.2)$$

with parameters $R_0 = 355.50$ MPa, $R_\infty = 368.72$ MPa and $b=31.75$ [-]. ϵ^{pl} is the equivalent plastic strain.

The APDL commands for material-force calculation are introduced as follows:

```
CINT,NEW,1
CINT,TYPE,MFOR
CINT,CTNC,CNodeComp
CINT,NCON,NumCon
CINT,NORM,0,2
CINT,SYMM,ON
```

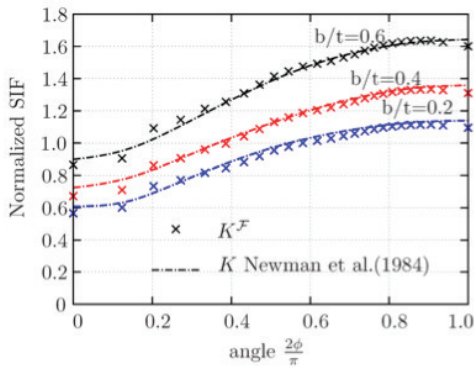


Figure 2.13. Comparison of normalized SIF through crack in elliptical crack front under remote tension

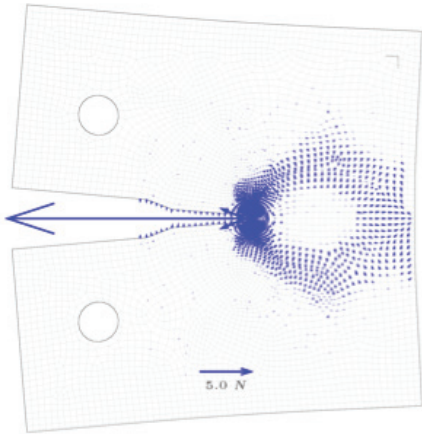


Figure 2.14. F^S distribution for compact tension specimen under displacement $u = 0.45$ mm

In case of plasticity, it is necessary to use a projection procedure of the internal variables, like plastic strain, equivalent plastic strain, etc., from the integration points to the nodes to compute the gradients of the variables at integration point (equation (A.14) in the appendix). ANSYS software uses the L_2 projection method with the global consistent matrix. The results shown in Figure 2.15 present the history of the loading versus material force and the experimental results for the separated energy release rates. For the sake of clarity, we plot both, close-field contour around the crack tip and far-field contour results. The total material force F underestimates the experimental results. This behavior might be interpreted as the energy consumed by the plastic dissipation in the fracture process zone. For further information on this case study, the reader is referred to Özenç et al. (2013).

Summary

Fracture mechanics-based modeling by using the finite element method is a nontrivial undertaking. Using a unique approach to the main fracturing phenomenon extremely important in engineering applications. The recently implemented material-force approach in ANSYS software offers a powerful tool for evaluating fracture criteria and crack propagation directions in fracture mechanics applications by the finite element method. This white paper illustrated the difference between mechanics in physical space and material space; furthermore, it presents information about what should be known to consider material forces as a fracture criterion and crack path predictor. The case studies demonstrate the general applicability of the approach and explain how the method can be used in ANSYS.

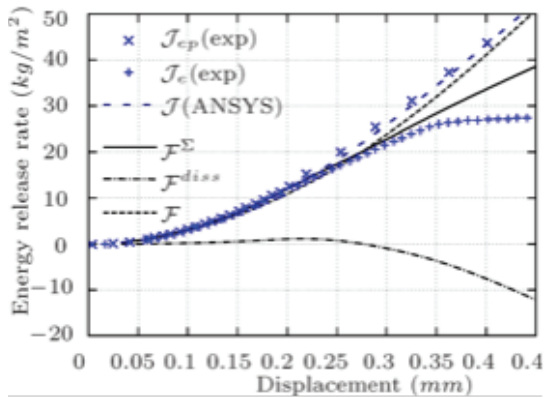
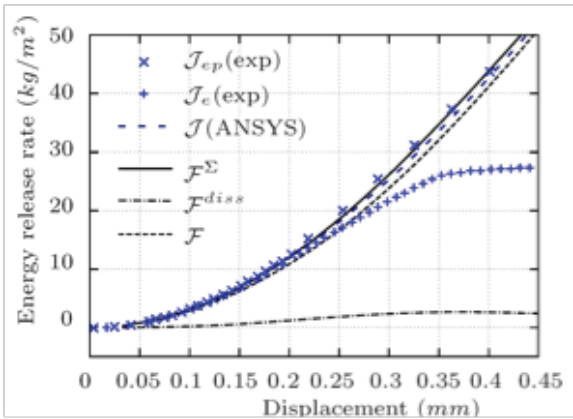


Figure 2.15. Comparison of energy release rate results obtained by different methods and experimental study versus displacements for close-field contour (top) and far-field contour (bottom)

Appendix Theory

A.1 Theory of Material-Force Approach

Contrary to physical forces, material forces act on the material space. Thus, they essentially represent the effects of discontinuities, such as inhomogeneities and imperfections. Based on mechanics in the material space, a concept of generalized forces acting on imperfections of crystals was first introduced by Eshelby (1951 and 1970). Although he used the term forces in singularity in his time, today they are commonly called material or configurational forces. The forces, introduced by Eshelby, can be interpreted as the representation of the negative gradient of the strain energy function with respect to the position of an imperfection. In this respect, in an elastic solid with a predefined crack, this explanation coincides with the J-integral in a vectorial setting in which its tangential component with respect to the crack surface represents the variation of the total dissipation of the configurational changes, since only energy dissipation exists because of the crack advancement.

In the work of Maugin and Trimarco (1997), the material force theory is developed within the context of large strain. A general application for a finite element implementation of material forces is presented by Braun (1997) and Steinmann (2000). Recently, the extension of the material-force approach to nonlinear and inelastic materials is treated by Näser et al. (2007 and 2009).

A.1.1 Material Forces in Elasticity

The framework of the material force approach is presented in a small strain description in which the displacement gradient ∇u is small enough compared to unity. Let the position of a material particle be denoted as $x \in B_x$ and the vector $u(x, t)$ is described as the corresponding displacement field on B_x , whereby t represents time. Furthermore, the displacement gradient can be introduced as $\nabla u = h$. According to this introduction, the strain tensor is $\epsilon = [h^{e}]^{sym}$. The free Helmholtz energy may be introduced as

$$\Psi = \Psi(\epsilon, X) \quad (A.1)$$

The material gradient of the assumed Helmholtz energy density yields

$$\nabla \Psi = \nabla \Psi(\epsilon, X) = \frac{\partial \Psi}{\partial X} \Big|_{exp} \quad (A.2)$$

in which the Cauchy stress tensor is $\sigma = \partial_\epsilon \Psi$. Additionally, using the additive properties of the small strain tensor leads to

$$\nabla \Psi = \nabla \Psi(\epsilon, \kappa, X) = \sigma : \nabla_X(\epsilon) + \frac{\partial \Psi}{\partial X} \Big|_{exp} \quad (A.3)$$

and, finally, by using differentiation by parts on $\sigma : \nabla \Psi(\varepsilon)$, we obtain the energy momentum balance

$$\nabla \cdot (\Sigma) = \frac{\partial \Psi}{\partial \mathbf{X}} \Big|_{exp}, \quad (\text{A.4})$$

in which $\Sigma = \Psi \mathbf{1} - \nabla u^t \sigma$ is the Eshelby stress tensor in a small strain theory. It is noted that $\nabla \sigma$ vanishes when no physical body forces are present.

A.1.2 Material Forces in Plasticity

According to the description in the previous section, the strain field description of associative elasto-plasticity can be assumed as an additive decomposition of the strain tensor into elastic and plastic parts as $\varepsilon = \varepsilon^e + \varepsilon^p$, in which $\varepsilon^e = [h^e]^{sym}$. Furthermore, the free Helmholtz energy may be introduced as

$$\Psi = \Psi(\varepsilon^e, \kappa, \mathbf{X}). \quad (\text{A.5})$$

Similar to the case of small strain elasticity, the full derivation of the material gradient of the assumed Helmholtz energy density yields

$$\nabla \Psi = \nabla \Psi(\varepsilon^e, \kappa, \mathbf{X}) = \sigma : \nabla \varepsilon^e + \frac{\partial \Psi}{\partial \kappa} \nabla_X \kappa + \frac{\partial \Psi}{\partial \mathbf{X}} \Big|_{exp}, \quad (\text{A.6})$$

in which κ is the equivalent plastic strain or the internal hardening variable, $\sigma = \partial_{\varepsilon^e} \Psi = -\partial_{\varepsilon^p} \Psi$ and $q = \partial_{\kappa} \Psi$. Additionally, using the additive properties of the strain tensor leads to

$$\nabla \Psi = \Psi(\varepsilon^e, \kappa, \mathbf{X}) = \sigma : \nabla(\varepsilon - \varepsilon^p) + \frac{\partial \Psi}{\partial \kappa} \nabla_X \kappa + \frac{\partial \Psi}{\partial \mathbf{X}} \Big|_{exp} \quad (\text{A.7})$$

and, by using differentiation by parts on $\sigma = \partial_{\varepsilon} \Psi$, we obtain the energy momentum balance

$$\nabla \cdot (\Sigma) = \sigma : \nabla_X \varepsilon^p + q \nabla_X \kappa + \nabla u^t \mathbf{b} + \frac{\partial \Psi}{\partial \mathbf{X}} \Big|_{exp}, \quad (\text{A.8})$$

in which $\Sigma = \Psi \mathbf{1} - \nabla u^t \sigma$ is the Eshelby stress tensor in a small strain theory.

A.1.3 Numerical Implementation

In the context of a finite element discretization, a straight-forward Galerkin discretization can be obtained by the variational format of the quasi-static energy momentum balance in which the domain is divided into the elements $\prod_{e=1}^{numel} \mathcal{B}^e \subset \mathcal{R}^3$. Therefore, each element geometry in Bx is

interpolated from nodal positions \mathbf{X} by shape functions N , respectively. This assumption leads to interpolated values of

$$\tilde{\mathbf{X}}_N = \sum_{n=1}^E N(\xi) \mathbf{X}_N \quad \text{and} \quad \tilde{\mathbf{x}}_N = \sum_{n=1}^E N(\xi) \mathbf{x}_N. \quad (\text{A.9})$$

In addition, the gradients on each element can be evaluated

$$\nabla \tilde{\kappa}_N = \sum_{n=1}^E \nabla N(\xi) \kappa_N. \quad (\text{A.10})$$

Here, the nodal information must be sufficiently smooth to allow the gradient to be meaningful. This requirement can be easily satisfied by C1-continuity and higher continuous interpolations. After the elementwise discretization of the virtual displacements, we end up with nodal material forces

$$\mathcal{F} = \prod_{e=1}^{numel} \int_{\mathcal{B}} [\boldsymbol{\Sigma} \cdot \nabla_X \mathbf{N} + (-\boldsymbol{\sigma} : \nabla_X \boldsymbol{\epsilon}^p + q \cdot \nabla_X \kappa) \mathbf{N}] dV, \quad (\text{A.11})$$

In which \mathcal{F} is the generalized material force that is energy-conjugated to the crack propagation rate, and we may split \mathcal{F} as

$$\mathcal{F} = \mathcal{F}^\Sigma + \mathcal{F}^{Diss}, \quad (\text{A.12})$$

in which

$$\mathcal{F}^\Sigma = \prod_{e=1}^{numel} \int_{\mathcal{B}} [\boldsymbol{\Sigma} \cdot \nabla_X \mathbf{N}] dV, \quad (\text{A.13})$$

and

$$\mathcal{F}^{Diss} = \prod_{e=1}^{numel} \int_{\mathcal{B}} [(-\boldsymbol{\sigma} : \nabla_X \boldsymbol{\epsilon}^p + q \cdot \nabla_X \kappa) \mathbf{N}] dV. \quad (\text{A.14})$$

It is noted that in elastic solids, equation (A.14) vanishes. Therefore, the crack driving force can be introduced as

$$\mathcal{F} = \mathcal{F}^\Sigma = \prod_{e=1}^{numel} \int_{\mathcal{B}} [\boldsymbol{\Sigma} \cdot \nabla_X \mathbf{N}] dV. \quad (\text{A.15})$$

The solution of equation (A.15) yields nodal material force vectors at the nodes. Generally, the value determined from the discrete force at the crack-tip node represents a significant part of the energy release rate. However, the value obtained from a domain evaluation yields a result close to the theoretical (target) value, shown in Tables 2.1 and 2.2



ANSYS, Inc.
Southpointe
275 Technology Drive
Canonsburg, PA 15317
U.S.A.

724.746.3304
ansysinfo@ansys.com

ANSYS, Inc. is one of the world's leading engineering simulation software providers. Its technology has enabled customers to predict with accuracy that their product designs will thrive in the real world. The company offers a common platform of fully integrated multiphysics software tools designed to optimize product development processes for a wide range of industries, including aerospace, automotive, civil engineering, consumer products, chemical process, electronics, environmental, healthcare, marine, power, sports and others. Applied to design concept, final-stage testing, validation and trouble-shooting existing designs, software from ANSYS can significantly speed design and development times, reduce costs, and provide insight and understanding into product and process performance. Visit www.ansys.com for more information.